Journal of
Computational and Theoretical Nanoscience
Vol. 4, 686–691, 2007

RESEARCH ARTICLE

Field Computations of Optical Antennas

Roman Kappeler[1, 4, *], Daniel Erni[1, 2], Cui Xudong[3], and Lukas Novotny[4]

[1] *Communication Photonics Group, Laboratory for Electromagnetic Fields and Microwave Electronics, ETH Zürich, Gloriastr. 35, 8092 Zürich, Switzerland*
[2] *General and Theoretical Electrical Engineering (ATE), Faculty of Engineering, University of Duisburg-Essen, Bismarckstr. 81, 47057 Duisburg, Germany*
[3] *Computational Optics Group, Laboratory for Electromagnetic Fields and Microwave Electronics, ETH Zürich, Gloriastr. 35, 8092 Zürich, Switzerland*
[4] *The Institute of Optics, University of Rochester, Rochester NY, 14627, USA*

Antenna-based near-field optical microscopy and spectroscopy makes use of locally enhanced optical fields created near laser-irradiated metal nanostructures acting as local probes. Using three-dimensional simulations based on the finite element method we study the electromagnetic fields near various optical antennas and we optimize their geometry in order to bring out a strong enhancement in a selected frequency range. Our results provide clear guidelines for the fabrication of efficient antenna structures and for improving the sensitivity of current near-field microscopy schemes.

Keywords: Optical Antennas, Near-Field Optical Microscopy, Surface Enhanced Spectroscopy, Plasmonics, Nanoparticles, Nanorods.

1. INTRODUCTION

Antennas are components to receive and transmit electromagnetic waves. Whereas antennas are primary devices in radio frequency applications for many years, the concept of optical antennas is relatively new. Analogously, optical antennas are components designed to transceive optical signals. The application range where optical antennas will be used is likely to become as wide as the one for the radio wave counterpart. Already an established application area for optical antennas is near-field optical microscopy and spectroscopy.[1] There the antenna efficiently converts the energy of an incident electromagnetic wave to highly localized energy. The antenna concept is used to increase the signal strength and the resolution but also to influence the radiative decay rates of sample molecules. In scanning near-field optical microscopy (SNOM), the optical antenna often consists of a sharp noble metal tip, which is illuminated by a laser beam. The tip localizes the energy of the incoming laser beam such that light is concentrated to a highly localized area whose dimensions are essentially defined by the sharpness of the tip (currently down to 10 nm). The underlying physical effects are manifold and often hard to determine: static effects such as the lightning rod effect as well as dynamic effects such as surface plasmon polariton (SPP) resonances contribute to the antenna behavior. For example, according to the lightning rod effect, any sharp geometry should yield high electrical fields, but in practice only about half of the tips show a good electrical field enhancement even if they are equally sharp. Additionally, the field enhancement depends on the local environment, on the tip shape and also on the experiment itself (illumination conditions). Recent single molecule fluorescence experiments are very indicative for these challenges:[2] etched gold tips were found to provide weak fluorescence enhancement because of the predominating effect of fluorescence quenching at short distances. A good optical antenna has to provide a strong local field enhancement and low energy dissipation. Currently, good optical antennas for fluorescence applications are provided by colloidal gold particles attached to the end of an etched glass fiber tip. But the field localization and the magnitude of the field enhancement are modest. Anger et al.[2] have measured the total fluorescence dependence on the probe–molecule distance. As the distance is reduced, the fluorescence rate first increases due to the field enhancement effect and then, at distances smaller than ∼5 nm, drops because of nonradiative energy transfer to the particle. To improve the field enhancement, spheroids or nanorods can be used. As shown later, a nanorod behaves like a downscaled dipole antenna known from classical antenna theory. However, at optical frequencies the properties of metals are significantly different from their behavior at radiowave or microwave frequencies. Rather than being characterized

*Author to whom correspondence should be addressed.

 1546-198X/2007/4/686/006 doi:10.1166/jctn.2007.033

by an instantaneous response to the driving external field the electrons in the metal behave like a plasma confined by the particular geometry of the metal's boundaries. Consequently, the resonances of an optical antenna made of real metals are red-shifted with respect to the resonances of a perfect metal. Mühlschlegel et al.[3] have investigated the resonance of gold dipole antennas. The antenna length at resonance has been found to be considerably shorter than one-half of the excitation wavelength. The strongest field can be found in the feed gap of the dipole antenna. A similar antenna structure is the bow-tie antenna, which has been recently studied by Schuck et al.[4] The sharp edges lead to an even better confinement of the light in the center of the structure. The same structure has been integrated on the facet of a commercial diode laser by Cubukcu et al.[5] for the purpose of a plasmonic laser antenna. However, for SNOM an antenna is needed, where the maximum electrical field is located at the apex of an optical probe. Using this constraint, we investigate different strategies to achieve a strong local field enhancement. All the simulations and results presented in this article have been performed using COMSOL multiphysics, a software toolkit based on the finite element method (FEM).

2. GOLD NANOPARTICLES

Because of its simple geometry a metal particle is a simple prototype antenna. Analytical solutions are known and quantitative comparisons with experimental data are straightforward. The scattering of light by a dielectric sphere has first been solved analytically by Mie.[6] For small particles (in the quasi-static limit), the external electrical field distribution can be described by the fields of a dipole located at the center of the sphere.[7] The total electric field can be given as a superposition of the incident field and the scattered field using the dipole approximation[8]

$$E_{\text{tot}} = E_0 + \frac{\omega^2 e^{-ika}}{k^2}\varepsilon_0 \frac{\varepsilon - 1}{\varepsilon + 2} E_0 \tag{1}$$

where ε is the complex permittivity. For all calculations ε has been taken from Johnson and Christy.[9] Because of the existence of an analytical solution for this problem, the system is perfectly suitable for a validation of the numerical approach used in this study. We find that the numerical FEM results are in nearly perfect agreement with the analytical solution (1) and hence the FEM code can be reliably applied to more complex antenna structures. For an excitation wavelength of $\lambda = 650$ nm the maximum intensity enhancement at the surface of the sphere is found to be $\sim$12.5.

In a next step we have introduced a second sphere at variable distance to the first one. Compared to the field enhancement of a single sphere, much stronger enhancements are found in the gap between the two spheres. Furthermore, the resonance shifts to the red. We have investigated both separated and intersecting spheres. As shown by the charge distributions in Figure 1 there is an important difference between these two cases: a single dipole is induced in the connected structures, whereas in the latter case, a dipole is induced in each individual sphere. The induced dipoles of the two separated spheres interact and because the charges are of different sign on the surfaces of closest proximity the spheres experience a mutual attractive force. The high surface charge density yields to crowding of electrical field lines between the two spheres and hence the field enhancement of closely spaced spheres becomes very strong.

For the other case of two interconnected spheres only a single dipole is induced over the whole structure. A consequence thereof is a much longer resonance wavelength compared to the case of two separate spheres.[10] Interestingly, a singularity in the electrical field distribution can be found at the edges of the indent, which leads to a discontinuity of the surface charge density and hence to extremely high fields. By choosing spheres of different sizes an asymmetry can be introduced giving rise to a displacement of the electric field distribution towards the smaller sphere (c.f. Fig. 1). Although a high ratio of the radii leads to a high ratio of electrical field enhancements at the two sphere ends, the maximum field intensity tends to decrease as the size difference between the spheres increases. The overlap distance also influences the total electrical field enhancement. We have found the highest field strengths for an overlap distance of 1.4 nm. By varying the radii and the overlap distance, the total length changes and hence the resonance wavelength shifts to the blue. However, the resonance wavelength also depends on other parameters, such as the sphere radii and the overlap distance.

3. SELF-SIMILAR ANTENNA

By generalizing the asymmetric two-sphere antenna to multiple spheres we can obtain a self-similar antenna. Li, et al.[11] already proposed a self-similar arrangement of spheres for enhancing and localizing optical fields. A self-similar antenna can be constructed according to

$$r_1 = \kappa r_0 \tag{2}$$

$$d_1 = \kappa d_0 \tag{3}$$

where κ is the scaling constant and r_0, r_1 are the radii of two adjacent spheres. The design of Li et al. uses a positive overlap parameter d, whereas in our design the parameter d is negative. A multiplying effect can be observed for the self-similar lens: each sphere is excited by the near-field of an adjacent larger one. To first approximation, the influence of the smaller sphere on the next larger sphere can be neglected (the smaller κ, the better the approximation). The incident electrical field for the small sphere is the sum of the field of the incident electromagnetic wave

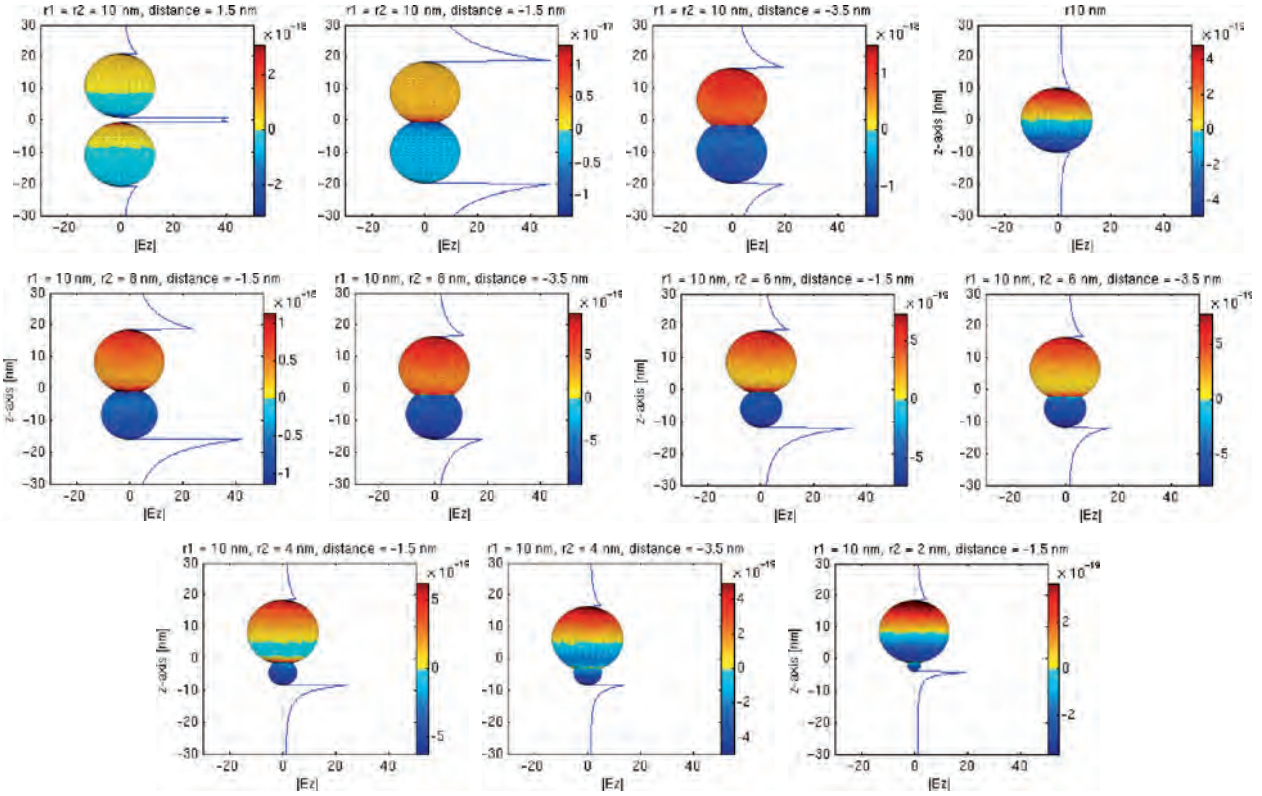

Fig. 1. Surface charge density and the field distribution along the symmetry axis are depicted for various arrangements of two spheres excited at resonance. The overlap distance increases from left to right and the radius of the second sphere is decreased from the top to the bottom.

and the near-field of the next larger sphere. However, this simple picture has its obvious limitations: the model predicts equal field strengths on both ends of the smallest and foremost sphere but calculations show that the strongest field is concentrated in the gap between the smallest and the next larger sphere.

Figure 2 shows the field distribution of a self-similar antenna made of three penetrating spheres (negative d). It can be seen, that the highest electrical field can be found at the apex—a key requirement for near-field optical imaging. Another perspective is provided by the surface charge density plotted in Figure 3 for two different self-similar

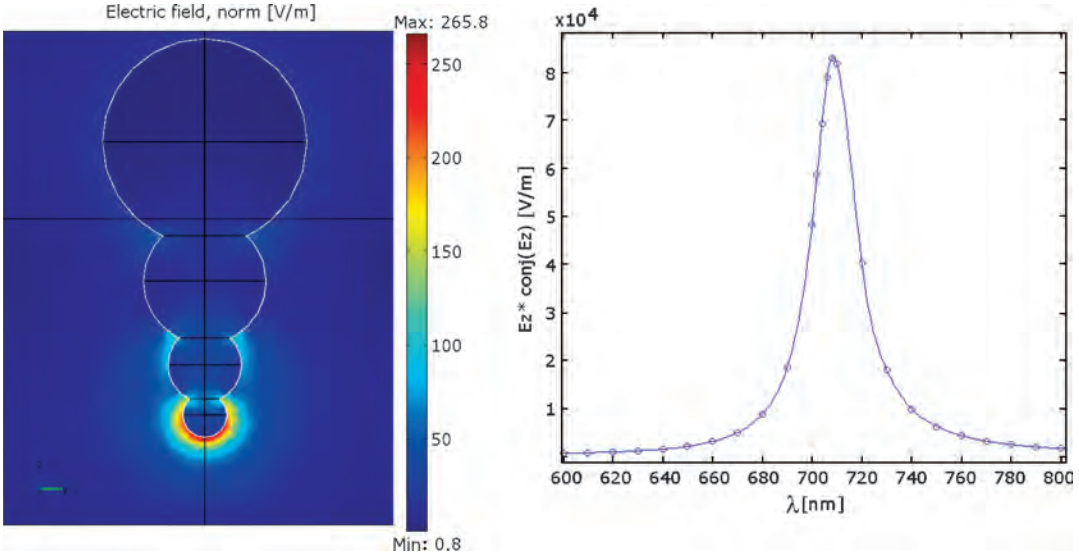

Fig. 2. Left: the field strength (|E|) is plotted for the resonance condition $\lambda = 708$ nm for a self-similar antenna based on four gold spheres ($r_0 = 10$ nm, $d_0 = 1.5$ nm, $\kappa = 0.7$). Right: the maximum field enhancement (at the surface of the smallest sphere on the z-axis) is plotted versus the excitation wavelength for the self-similar antenna depicted on the left.

antennas. The outermost spheres are either only positively or negatively charged, respectively. Hence the overall behavior is dipole-like. Again, the sharp concave edges lead to a discontinuity of the surface charge distribution and to an additional superimposed charge separation. These charges are polarized in opposite to the charge separation imposed by the dipole of the outermost spheres.

Because of the lightning rod effect it appears that highest field enhancements are obtained for small apex radii. However, for a sphere-pair with a large size ratio the coupling becomes very ineffective (c.f. Fig. 1). We have found good coupling behavior for $\kappa = 0.7$. Hence, intermediate spheres assume the function of coupling elements from the largest to the smallest sphere.

Hafner et al.[12] and Esteban et al.[13] proposed an optical antenna in the form of a conical particle as shown in Figure 4. The geometry is similar to the self-similar antenna shown in Figure 2, except that the notches were removed. We have compared the two antennas and found a maximum electrical field enhancement of ∼135 for the conical antenna and 270 to 1180 for the self-similar antenna. Apparently, by adding notches to the conical antenna the electrical field enhancement can be improved. The reason for this is the additional charge separation at the notches (refer text above). It can be shown that the field strength in the notches becomes singular if the notches possess perfect edges. This singular behavior is fatal for obtaining a reliable absolute value for the electrical field enhancement by means of simulation. The more the resolution is increased, the higher are the obtained fields in the notches. We have simulated the structure with different software tools based on different methods and a similar behavior can be observed for all of them. Because these intrusion singularities are not easy to handle, the self-similar antenna provides a benchmark model for comparing different numerical methods. While it is difficult to determine an exact value for the field enhancement for a given self-similar antenna, the spectral position of the resonances are not as strongly affected by geometrical variations.

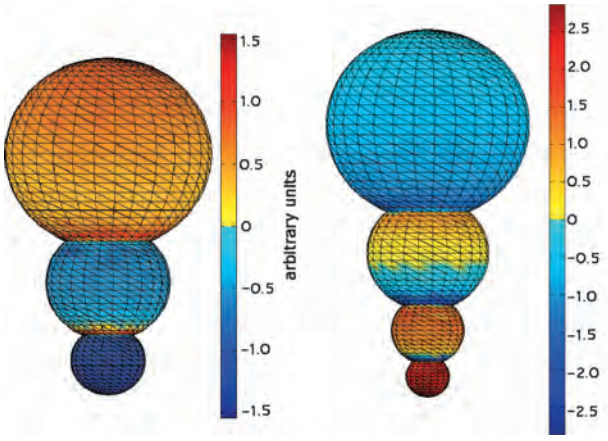

Fig. 3. Plots of the surface charge density show that the overall behavior of the self-similar antenna is dipole-like. However, other inverted dipoles are created by the notches between adjacent spheres. Note that the surface charge density is not symmetrically distributed on the spheres, but is larger on smaller spheres. This yields a high electrical field at the apex of the antenna.

For the self-similar antenna shown in Figure 2 we have calculated a resonance wavelength of $\lambda_{res} = 708$ nm, whereas the resonance wavelength for the conical particle antenna is $\lambda_{res} = 610$ nm. Evidently, the resonance wavelength is considerably longer for the self-similar antenna compared with the conical particle despite of the fact that both antennas have the same height. The longer resonance wavelength of the self-similar antenna is a direct consequence of the notches which increase the effective surface path from the top to the end (apex). Higher-order multipoles have only a minor influence on the resonance condition and generally tend to shift the resonances towards the blue.

Alluding to Boyd et al.,[14] the local enhancement factor L may be written as a product of factors denoting the lightning rod effect L_{LR}, quasi-static considerations L_{QS}, and the plasmon resonance L_{SPPR}:

$$L = L_{LR} L_{QS} L_{SPPR} \tag{4}$$

In order to obtain high field enhancements all these factors need to be maximized for a given frequency. However, for metal structures with dimensions that are smaller than the skin-depth of the metal (e.g., apex of antenna) the lightning-rod effect becomes a secondary effect and the optical response is dominated by plasma resonances of the free-electron gas.

4. SILVER SPHERES PROTECTED BY A GOLD COATING

In the quasi-static regime, the plasmon resonance of a spherical particle is simply determined by the singularities of the particle's polarizability

$$\alpha = 4\pi a^3 \varepsilon_0 \frac{\varepsilon_{metal} - \varepsilon_{insulator}}{\varepsilon_{metal} + 2\varepsilon_{insulator}} \tag{5}$$

For silver particles in air the plasmon resonance is near $\lambda_{res} = 370$ nm. Our simulations for self-similar antenna structures have revealed that the resonance wavelengths shifts towards the red as the effective length of the antenna is increased. Thus, fusing different sized silver particles together allows the resonance to be shifted from the UV into the visible. Unfortunately, silver is a chemically unstable material and its surface needs to be protected with a chemically inert layer. A chemical procedure for covering a gold sphere with silver has been worked out[15] and it is intuitive that a similar procedure can be developed for covering silver particles with chemically-inert gold layers. To understand the consequence of such a protection layer on the optical response of the antenna we have calculated the plasmon resonances of a simple silver sphere for different thicknesses of a protecting gold layer.

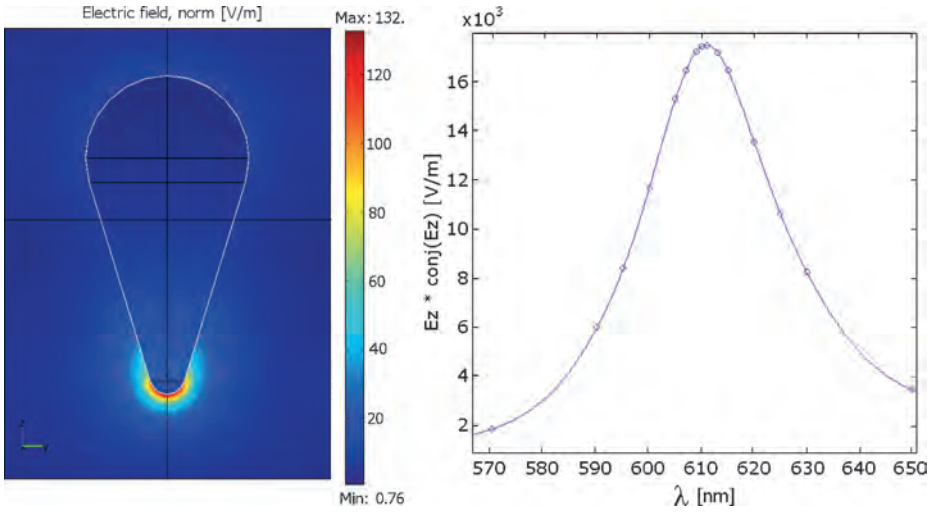

Fig. 4. Field distribution and field enhancement for a conical particle antenna. This geometry is derived from the self-similar antenna calculated in Figure 2 by removing the notches. The graph shows the maximum of the electrical field (at the apex of the antenna) plotted versus the wavelength of the incident field. Note that compared to the self-similar antenna discussed in Figure 3 the resonance of the conical particle antenna is blue-shifted by almost 100 nm.

The simulation results are presented in Figure 5. Interestingly, although the silver core is now surrounded by a gold layer the resonances are still defined by the silver–air interface. However, the thicker the gold coating the weaker is the silver resonance. As the gold layer thickness increases a new resonance emerges. This resonance originates from the gold–air interface and because of the stronger interband damping in gold the new plasmon resonance is much weaker than the one of the silver particle. It is interesting to note that the resonance wavelengths are not affected by the layer thickness and similar results have been found for silver coated gold particles.[15]

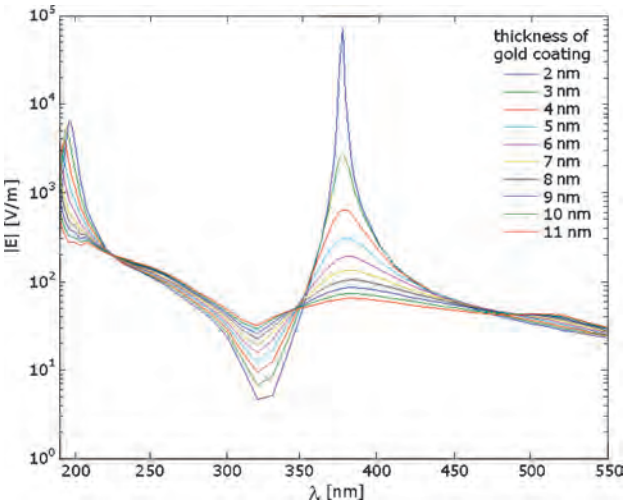

Fig. 5. Field enhancement of a 40 nm silver particle coated with gold layers of variable thicknesses. Interestingly, the resonance wavelength of the silver particle is not affected by the gold layer although the surface of the silver particle is no longer surrounded by air but by gold. The thicker the gold coating gets, the weaker is the silver resonance and the stronger is the gold resonance at 530 nm.

5. NANORODS

The simplest radiowave antenna is the $\lambda/2$ dipole or wire antenna. The resonances for the $\lambda/2$ dipole can be described according to

$$l = \left(n + \frac{1}{2}\right)\lambda \tag{6}$$

To study the optical antenna behavior beyond the quasi-static regime we have calculated the response of gold nanorods of a total length of 220 nm and 20 nm diameter. In Figure 6(a) the electric field enhancement at the apex is plotted versus the excitation wavelength. Field distributions for the maxima appearing in the spectrum are plotted in Figure 6(b). These modes correspond to the principal resonances of a wire antenna. Using Eq. (6), the $\lambda/2$ mode is expected to be at a wavelength of 440 nm. Instead, we find the $\lambda/2$ mode to be at 1298 nm for the gold nanorod. The origin of the discrepancy lays in the assumptions inherent in Eq. (6): negligible thickness and a perfect conductivity. None of these assumptions holds for the gold nanorod. In the visible, gold is not a good conductor and, compared to the length of the wire, the thickness is not negligible. Nevertheless, a resonance shift from 440 nm to 1298 nm is rather unexpected.

Calander and Willander[16] have carried out detailed calculations for silver and gold spheroids of 100 nm, 200 nm, 300 nm, and 400 nm total length. While a spheroid and a nanorod are different geometries they can both be employed as models for a traditional wire antenna. For a gold spheroid of 200 nm height and an aspect ratio of 11 Calander and Willander find a resonance wavelength of roughly 1150 nm which lies in the same range as the resonance wavelength we have determined for the nanorod. The higher the aspect ratio, the larger is the field enhancement. This may be partially due to the fact, that

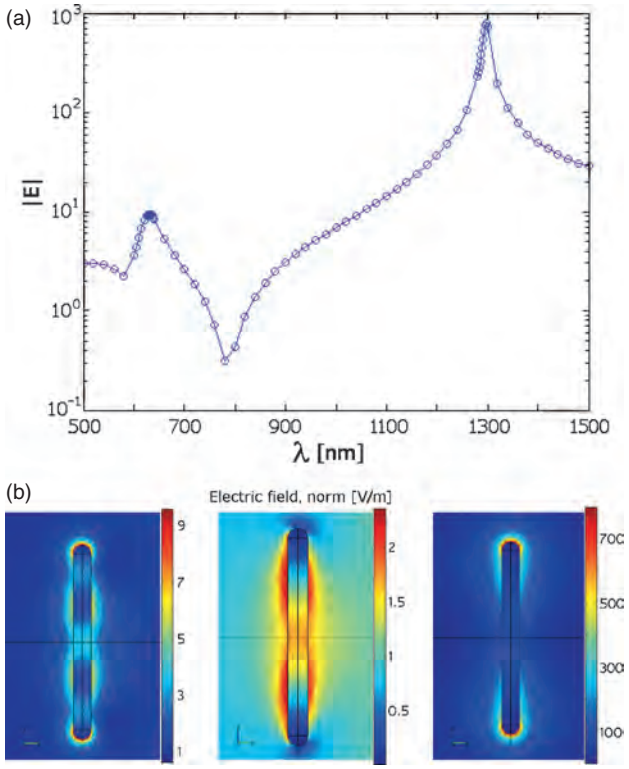

Fig. 6. (a) Spectral dependence of the field enhancement at the apex of a 220 nm gold nanorod of 20 nm diameter. (b) Field distributions for the wavelengths corresponding to the three extrema of the curve in (a). For $\lambda \sim 1300$ nm the field distribution (right) corresponds to the $\lambda/2$ mode. The mode at $\lambda \sim 650$ nm (left) is the $3\lambda/2$ mode, and the 'dark' mode at $\lambda \sim 780$ nm (center) corresponds to the symmetric λ-mode.

the apex radius ($r = b^2/2a$) is smaller for higher axial ratios and the lightning rod effect increases the local field strength. On the other hand, for the nanorod we observe that the field enhancement is larger for long nanorods independent of the apex radius.

6. CONCLUSIONS

We have shown that structured tips such as a self-similar arrangement of penetrating spheres provide efficient optical antennas for near-field optical microscopy and spectroscopy. We have investigated the influence of plasmon resonances in both the quasi-static regime and in the retarded regime. We find that the highest enhancements are obtained in the retarded regime, i.e., when the antenna design is related to an effective wavelength. Similar to the gold and silver spheroids investigated by Calander and Willander,[16] we have observed a dramatically shifted resonance wavelength for nanorods compared to classical antenna theory. The most important factors for the field enhancement are surface plasmon resonances. We find that the resonance wavelength λ_{res} of an antenna with effective length L is shifted to the red by a factor n_{res} according to

$$\lambda_{res} = \lambda_o n_{res} \tag{7}$$

where λ_o is the resonance wavelength of an antenna made of a perfect metal. For a nanorod, $\gamma = 2\pi n_{res}/\lambda$ with λ being the free-space wavelength, corresponds roughly to the propagation constant of the TM_{01} waveguide mode propagating along an infinite wire.[17] The factor n_{res} can be understood as an effective surface index of the wire.[18] Thus, while n_{res} varies from antenna to antenna, the index makes it possible to directly downscale traditional antenna designs into the optical regime.

References

1. N. Anderson, A. Bouhelier, and L.Novotny, *J. Opt. A: Pure and Appl. Opt.* 8, S227 **(2006)**.
2. P. Anger, P. Bharadwaj, and L. Novotny, *Phys. Rev. Lett.* 96, 113002 **(2006)**.
3. P. Mühlschlegel, H. Eisler, O. Martin, B. Hecht, and D. Pohl, *Science* 308, 1607 **(2005)**.
4. P. J. Schuck, D. P. Fromm, A. Sundaramurthy, G. S. Kino, and W. E. Moerner, *Phys. Rev. Lett.* 94, 017402 **(2005)**.
5. E. Cubukcu, E. Kort, K. Crozier, and F. Capasso, *Appl. Phys. Lett.* 89, 093120 **(2006)**.
6. G. Mie, *Ann. Phys. Leipzig* 25, 377 **(1908)**.
7. M. Born and E. Wolf, Principles of Optics, 7th edn. Cambridge University Press **(1999)**.
8. L. Novotny and B. Hecht, Principles of Nano-Optics, Cambridge University Press **(2006)**.
9. P. B. Johnson and R. W. Christy, *Phys. Rev. B* 6, 4370 **(1972)**.
10. I. Romero, J. Aizpurua, G. Bryant, and F. Garcia de Abajo, *Opt. Express* 14, 9988 **(2006)**.
11. K. Li, M. Stockman, and D. Bergman, *Phys. Rev. Lett.* 91, 227402 **(2003)**.
12. Ch. Hafner and J. Smajic, Maxwell Solvers for Opitcs, Handbook of Theoretical and Computational Nanotechnology, edited by Michael Rieth and Wolfgang Schommers, American Scientific Publishers, Stevenson Ranch, CA **(2006)**, Vol.1.
13. R. Esteban, R. Vogelgesang, and K. Kern, *Nanotechnology* 17, 475 **(2006)**.
14. G. Boyd, Th. Rasing, J. Leite, and Y. Shen, *Phys. Rev. B.* 30, 519 **(1984)**.
15. N. R. Jana, *Roy. Soc. Chem.* 128, 954 **(2003)**.
16. N. Calander and M. Willander, *J. Appl. Phys.* 92, 4878 **(2002)**.
17. L. Novotny and Ch. Hafner, *Phys. Rev. E* 50, 4094 **(1994)**.
18. M. I. Stockman, *Phys. Rev. Lett.* 93, 137404 **(2004)**.

Received: 26 October 2006. Accepted: 30 October 2006.